Constant Elevation-Beamwidth Beamforming with Concentric Ring Arrays

Orel Peretz, Israel Cohen, *Fellow, IEEE,*

***Abstract*—A hybrid approach is proposed to efficiently design a constant elevation-beamwidth beamforming with concentric ring arrays (CRAs). The design exploits the degrees of freedom of the array geometry for superior performance. In particular, the ring radii and the beamformer coefficients are optimized simultaneously for all frequencies. We introduce a convex quadratic programming problem for a given CRA configuration, directly optimizing the beamformer coefficients while maintaining constant elevation-beamwidth over a wide range of frequencies. The proposed objective function contains a control variable, allowing a tradeoff between the directivity factor and the white noise gain. Subsequently, a hybrid approach is proposed to optimize the ring radii with a genetic algorithm exploiting the partial convexity of the problem. Experimental results demonstrate the flexibility and advantages of the proposed approach compared to the state-of-the-art in terms of directivity factor, white noise gain, sidelobe level, and beamwidth consistency, with reduced resources and a significantly lower computation time.**

***Index Terms*—Array processing, microphone array, concentric ring array, constant-beamwidth beamforming, frequency-invariant beamforming.**

I. Introduction

BEAMFORMING is a classical method for spatial filtering of a desired signal from noise and interference using observations from multiple microphones [1]–[3]. It has been at the forefront of research activity for many decades, applied in applications such as hands-free audio communication, hearing aids, and teleconferencing systems [4], [5]. Most applications involve signals that are broadband in nature in a three-dimensional (3D) setting, requiring efficient solutions for low latency, minimum resources, and high performance.

Conventional beamforming suffers from beamwidth narrowing as frequency increases, causing an undesired distorted low-passed output for signals deviating from the look direction. Over the last few decades, several frequency-invariant (FI) and constant-beamwidth (CB) methods have been suggested with different array geometries, which can be generally divided into three categories: linear [6]–[10], planar [11]–[24] and volumetric [25], [26]. The planar arrays are favored over the others due to their 2D steering ability and limited resources (area, number of elements, etc.). Among the planar array, geometries are: the rectangular arrays (RAs) [11]–[17], [27], the circular arrays (CAs) [18]–[20] and the concentric circular arrays (CCAs) [21]–[24]. The last is preferred in many applications due to 360° azimuth coverage and superior performance in direction of arrival (DoA) [21], [28], peak sidelobe level (PSLL) [29], noise suppression [30], and frequency invariance over a wide range of frequencies [31]. However, most works restrict the desired signal DoA to the horizontal plane, affecting the beamformer's performance in terms of directivity factor (DF) and white noise gain (WNG). In [32], a CB beamformer for CCAs controlling both the azimuth and elevation beamwidths was suggested. Yet, for large arrays, the computational complexity and required resources may be too high due to the large number of degrees of freedom (DOF). A compromise is the concentric ring array (CRA), where all microphones in a ring share the same weight. While eliminating beam steering ability, the number of DOFs is reduced, as are the computational complexity and required resources. In [33], a window-based CB beamformer for uniformly spaced CRA was suggested.

Generally, two main design controls are affecting the performance of the CRA beamformer: the ring radii and weights. Previous work on beampattern synthesis of CRAs optimizing both radii and weights includes optimization methods such as particle swarm optimization (PSO) [34], compressed sensing (CS) [35], and moth flame optimization (MFO) [36]. Yet, for the most part, these methods are computationally exhaustive for large arrays. Following, hybrid approaches [37]–[39] decomposing the optimization problem into two parts were suggested. In [37], a combination of a genetic algorithm (GA) and convex programming (CP) was proposed, exploiting the convexity of the problem and the parallelism of the GA for improved efficiency. Yang et al. [39] employed the same combination while optimizing the ring partitions in addition to the radii and weights under linear constraints. Unfortunately, all the aforementioned approaches were designed for the narrowband case without beamwidth control. Moreover, they ignore important performance measures such as the DF and WNG.

Recently, Klieman et al. [40] proposed a maximum DF CB beamformer with time-domain implementation by solving a mixed integer quadratic programming (MIQP) problem of both the weights and radii. However, it suffers from several disadvantages. First, the radii are optimized on a grid, which is computationally exhaustive, especially for a large grid. Second, the algorithm comprises two separate optimization problems: one for finding the weights that maximize the DF and the other for finding the finite impulse response (FIR) coefficients approximating the beamformer weights concerning the least-squares cost. Next, the FIR coefficients are designed independently for each ring. Consequently, the final time-domain solution is suboptimal, which may cause a degradation in performance. Lastly, objective function weighting and a pre-

The authors are with Andrew and Erna Viterbi Faculty of Electrical and Computer Engineering, Technion – Israel Institute of Technology, Haifa 3200003, Israel (e-mail: peretz.orel@campus.technion.ac.il; icohen@ee.technion.ac.il).

This research was supported by the Israel Science Foundation (grant no. 1449/23) and the Pazy Research Foundation

processing step are needed to compensate for the non-smooth filter response of the incoherent solution. How to design an efficient CB FIR beamformer with CRAs is still an open question. Moreover, to our knowledge, no hybrid approach has been developed for CB FIR-beamforming with CRAs.

In this paper, we propose an efficient approach for the design of a CB FIR beamformer with CRAs. The design exploits the degrees of freedom of the array geometry for superior performance. In particular, the ring radii and the FIR beamformer coefficients are optimized simultaneously for all frequencies. First, we utilize the continuous-phase representation of the FIR filters for defining a convex quadratic programming (CQP) problem, maintaining CB over a wide range of frequencies for a given CRA configuration. We propose an objective function that includes a control variable, allowing a tradeoff between DF and WNG. Following, a hybrid approach is proposed to optimize the ring radii with a genetic algorithm utilizing the aforementioned convex problem as its cost and exploiting the partial convexity of the problem. Simulation results compare the proposed approach against the state-of-the-art, showing several advantages. First, the flexibility of the proposed approach is demonstrated, allowing a compromise between DF and WNG. Second, the improved performance in terms of WNG, beamwidth consistency, and sidelobe level (SLL) due to the direct and joint optimization of the coefficients is shown. Lastly, the significantly lower computational time and faster convergence of the proposed approach are demonstrated through independent Monte Carlo (MC) runs.

Our motivation arises from many multi-speaker applications involving large spaces with speakers distributed across different pre-defined areas such as auditoriums, classrooms, houses of worship, and conference centers. In such scenarios, our beamformer with the eliminated steering ability can be installed as a circular ceiling array over the different regions of interest. This solution benefits from low cost, latency, and high performance [33].

The rest of the paper is organized as follows: Section II presents the CRA and signal model, problem formulation, and performance measures. In Section III, we introduce the proposed hybrid approach. Section IV presents experimental results, and in Section V, we summarize and highlight our conclusions.

Notation: Throughout the paper, the following notation is adopted: $\mathbf{X}$ is a matrix, $\mathbf{x}$ is a vector and x is a scalar. The i,j-th element of a matrix $\mathbf{X}$ is denoted $(\boldsymbol{X})_{i,j}$. The imaginary unit is j (so that $j^2 = -1$). The conjugate transpose of a matrix is $(\cdot)^H$, its conjugate is $(\cdot)^*$ and its transpose is $(\cdot)^T$. The Euclidean norm is $\|\cdot\|_2$. The $N \times N$ identity matrix is $\boldsymbol{I}_N$ and the $N \times 1$ all-ones vector is $\mathbf{1}_N$. The ceil of a number α is written as $\lceil \alpha \rceil$. Functions are denoted by lowercase italics, e.g., $f(\cdot)$. $\mathrm{Re}\{\cdot\}, \mathrm{Im}\{\cdot\}$ denote the real and imaginary parts of a complex scalar, vector, or matrix. The Kronecker product is denoted by $\otimes$, and the Hadamard product by $\circ$. Finally, the phase of the complex-valued variable α is denoted by $\angle\{\alpha\}$.

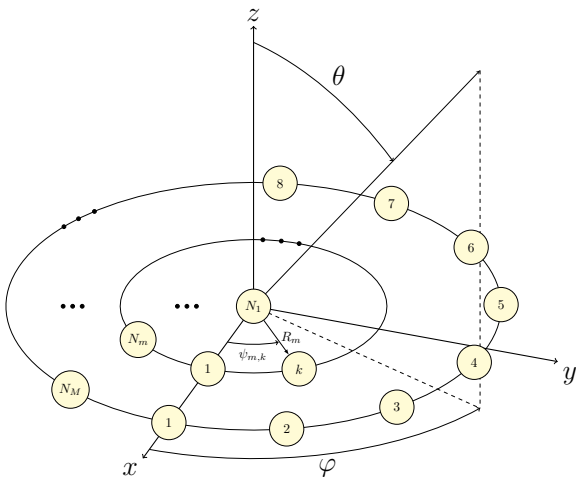

Fig. 1. *Illustration of a CRA with M rings and N_m microphones per ring.*

II. Problem Formulation and Performance Measures

A. Concentric Ring Array

Consider a discrete CRA with M rings. The m-th $(m = 1, ..., M)$ ring has a radius R_m, containing N_m equally spaced omnidirectional microphones, as illustrated in Fig. 1. We assume that the center of the CRA coincides with the first ring having $R_1 = 0$ and $N_1 = 1$. The total number of microphones in the array is $N = \sum_{m=1}^{M} N_m$.

The location of the k-th $(k = 1, ..., N_m)$ microphone on the m-th ring is given by

$$\boldsymbol{r}_{m,k} = R_m \left(\cos\psi_{m,k}, \sin\psi_{m,k}, 0\right)^T \tag{1}$$

$$\psi_{m,k} = \frac{2\pi\left(k-1\right)}{N_m} \tag{2}$$

where $\psi_{m,k}$ is the angular position, measured anti-clockwise concerning the x-axis.

To prevent spatial aliasing, the inner-microphone spacing on each ring should satisfy the Nyquist spatial sampling criterion, i.e., be less than $\lambda_m^{min}/2$, where λ_m^{min} is the minimal wavelength in which the m-th ring is effective in the beamforming process. Consequently, the number of microphones of the m-th ring is given by

$$N_m \geq \left\lceil \frac{4\pi R_m}{\lambda_m^{min}} \right\rceil . \tag{3}$$

Since the microphones are spaced uniformly and satisfy the Nyquist criterion, we get an azimuth-invariant beampattern. Therefore, without loss of generality, we choose $\varphi = 0$ for the rest of the paper.

B. Signal Model

Suppose a desired broadband signal $s(t)$ propagates in an anechoic acoustic environment at the speed of sound, i.e., $c = 340$ m/s, impinges on the CRA. We assume a far-field model so the wave can be approximated as planar. The DoA of the desired signal is parameterized by the elevation angle θ_d.

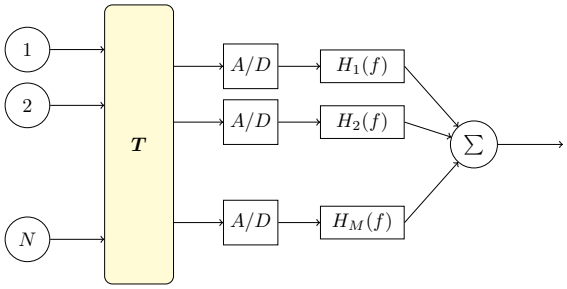

Fig. 2. *Block diagram of CRA FIR-beamformer.*

The signal observed by the m,k-th microphone is a time-delayed version of the original signal corrupted by noise $v_{m,k}(t)$, that is

$$x_{m,k}(t) = s(t-\tau_{m,k}) + v_{m,k}(t) \tag{4}$$

$$\tau_{m,k} = \frac{R_m}{c}\sin\theta\cos(\psi_{m,k}) \tag{5}$$

where $\tau_{m,k}$ denotes the propagation time difference between the origin and the m,k-th microphone. Applying the Fourier transform translates the time delay $\tau_{m,k}$ to a phase shift $e^{-j2\pi f\tau_{m,k}}$, that is

$$X_{m,k}(f) = e^{-j2\pi f\tau_{m,k}}S(f) + V_{m,k}(f) \tag{6}$$

where f is the temporal frequency. In vector form, the observed signal of the m-th ring becomes

$$\begin{aligned}\underline{\boldsymbol{X}}_m(f) &= [X_{m,1}(f),...,X_{m,N_m}(f)]^T \\ &= \underline{\boldsymbol{d}}_m(f,\theta)S(f) + \underline{\boldsymbol{V}}_m(f)\end{aligned} \tag{7}$$

where the vector $\underline{\boldsymbol{V}}_m(f)$ is defined similarly to $\underline{\boldsymbol{X}}_m(f)$ and $\underline{\boldsymbol{d}}_m(f,\theta)$ is the steering vector of the m-th ring given by

$$\underline{\boldsymbol{d}}_m(f,\theta) = \begin{bmatrix} e^{j\frac{2\pi fR_m}{c}\sin\theta\cos(\psi_{m,1})} \\ \vdots \\ e^{j\frac{2\pi fR_m}{c}\sin\theta\cos(\psi_{m,N_m})} \end{bmatrix}. \tag{8}$$

Concatenating the M rings steering vectors yields the steering vector of the CRA, which is given by

$$\boldsymbol{d}(f,\theta) = \left[\underline{\boldsymbol{d}}_1^T(f,\theta),...,\underline{\boldsymbol{d}}_M^T(f,\theta)\right]^T. \tag{9}$$

C. Problem Formulation

In the proposed beamformer design, the first stage is the summation of all microphone signals of each ring followed by an A/D sampler per ring. Then, in the second stage, each output signal is filtered by an FIR filter. A block diagram of the proposed beamformer design is illustrated in Fig. 2. While eliminating beam steering ability, the proposed design requires fewer resources and simplifies the computational complexity. Mathematically, the sum operation can be represented by applying a partitioning preprocessing matrix T of size $N\times M$ to the digital signal, defined as

$$\boldsymbol{T} = \begin{pmatrix} \mathbf{1}_{N_1}/N_1 & \mathbf{0} & \cdots & \mathbf{0} \\ \mathbf{0} & \mathbf{1}_{N_2}/N_2 & \cdots & \mathbf{0} \\ \vdots & \vdots & \ddots & \vdots \\ \mathbf{0} & \mathbf{0} & \cdots & \mathbf{1}_{N_M}/N_M \end{pmatrix} \tag{10}$$

The weight vector at frequency f of the CRA rings is given by

$$\underline{\boldsymbol{h}}(f) = [H_1(f),...,H_M(f)]^T \tag{11}$$

where $H_m(f)$ is the FIR frequency response at frequency f applied to the m-th ring. Using (10), the weight vector at frequency f of the CRA microphones can be expressed as:

$$\boldsymbol{h}(f) = \boldsymbol{T}\underline{\boldsymbol{h}}(f) \tag{12}$$

D. Performance Measures

In this section, we define some relevant performance measures for deriving and analyzing the proposed beamformer.

The beampattern describes the sensitivity of the beamformer to a plane wave impinging on the array from different directions, defined as

$$\begin{aligned}\mathcal{B}[\boldsymbol{h}(f),\theta] &= \boldsymbol{h}^T(f)\boldsymbol{d}(f,\theta) \\ &= \sum_{m=1}^{M}H_m(f)\sum_{k=1}^{N_m}e^{j\frac{2\pi fR_m}{c}\sin\theta\cos(\psi_{m,k})}.\end{aligned} \tag{13}$$

When the Nyquist criterion in (3) is satisfied, the beampattern can be expressed using the beampattern of continuous rings

$$\mathcal{B}[\boldsymbol{h}(f),\theta] = \sum_{m=1}^{M}H_m(f)N_mJ_0\left(\frac{2\pi f}{c}R_m\sin\theta\right) \tag{14}$$

where J_0 is the zero-order Bessel function.

The (narrowband) WNG quantifies the robustness of the beamformer to imperfections, such as microphone noise, displacement, and mismatch, defined as

$$\mathcal{W}(f) = \frac{\left|\boldsymbol{h}^T(f)\boldsymbol{d}(f,\theta_d)\right|^2}{\boldsymbol{h}^T(f)\boldsymbol{h}(f)}. \tag{15}$$

where θ_d is the look direction. The broadband WNG is defined as

$$\mathcal{W} = \frac{\int_f\left|\boldsymbol{h}^T(f)\boldsymbol{d}(f,\theta_d)\right|^2df}{\int_f\boldsymbol{h}^T(f)\boldsymbol{h}(f)df}. \tag{16}$$

Another important measure is the (narrowband) DF, which quantifies how the sensor array performs in the presence of reverberation, defined as

$$\begin{aligned}\mathcal{D}(f) &= \frac{|\mathcal{B}(f,\theta_d)|^2}{\frac{1}{2}\int_0^\pi|\mathcal{B}(f,\theta)|^2\sin\theta d\theta} \\ &= \frac{\left|\boldsymbol{h}^T(f)\boldsymbol{d}(f,\theta_d)\right|^2}{\boldsymbol{h}^T(f)\boldsymbol{\Gamma}(f)\boldsymbol{h}(f)}\end{aligned} \tag{17}$$

which is the ratio between the array gain in the look direction θ_d and the average gain over all other directions. $\boldsymbol{\Gamma}(f)$ is the pseudo-coherence matrix whose elements are

$$[\boldsymbol{\Gamma}(f)]_{i,j} = sinc\left(\frac{2\pi f\left\|\boldsymbol{r}_i-\boldsymbol{r}_j\right\|_2}{c}\right) \tag{18}$$

where $\boldsymbol{r}_i,\boldsymbol{r}_j$ $1\le i,j\le N$ are the coordinates of the i and j microphones. The broadband DF is defined as

$$\mathcal{D} = \frac{\int_f\left|\boldsymbol{h}^T(f)\boldsymbol{d}(f,\theta_d)\right|^2df}{\int_f\boldsymbol{h}^T(f)\boldsymbol{\Gamma}(f)\boldsymbol{h}(f)df}. \tag{19}$$

III. The Proposed Hybrid Approach

In this section, we present a hybrid approach for the design of a CB FIR beamformer with CRAs. The proposed approach optimizes simultaneously the ring radii and the FIR coefficients. This problem is generally nonlinear and nonconvex; however, for fixed radii, the relationship becomes linear and can be solved as a convex problem. Therefore, we decompose the optimization problem into two parts: a global search optimization and a convex one, where the second is incorporated as the cost of the first.

In Section III-A, we formulate the optimization constraints and objective function regarding the FIR-beamformer coefficients. This optimization problem aims to design a CB beampattern for a given CRA configuration with flexible control of the DF and WNG. Following, in Section III-B, we incorporate the above optimization problem as the cost of a genetic algorithm.

A. Constant-Beamwidth Beampattern Design

The following subsections describe the main steps in the CB FIR-beamformer design for a given CRA configuration: In Section III-A1, the continuous-phase representation is used to define the optimization problem in terms of the FIR coefficients. Next, the optimization constraints maintaining CB are defined in Section III-A2. Finally, in Section III-A3, an objective function is suggested that allows a tradeoff between WNG and DF.

1) Time Domain Filter Design: Implementing a broadband beamformer in the time domain is essential for applications requiring computational efficiency and low latency [41]. The FIR frequency response $H_m(f)$ is defined as

$$H_m(f) = \sum_{n=0}^{L} b_{n,m} e^{-j2\pi f n} \tag{20}$$

where $\{b_{n,m}\}_{n=0}^{L}$ are the real-valued coefficients of the m-th ring and L denotes the order of the filter. The design of an FIR filter is done by computing the optimal impulse response coefficients $\{b_{n,m}\}_{n=0}^{L}$ concerning a chosen performance measure. In many applications, such as speech, filtering the signal without distortion is desirable. This is why linear phase filters are preferred, as their linear phase characteristic introduces a pure time delay. The frequency response $H_m(f)$ can be expressed as

$$H_m(f) = A_m(f)\, e^{j\phi_m(f)} \tag{21}$$

where $A_m(f)$ is a real-valued amplitude function and $\phi_m(f)$ is continuous phase. This form is called a continuous-phase representation and is very common in filter design.

We design the filters as Type-I linear-phase FIR filters with even order and symmetric coefficients. All filters have the same order to maintain a fixed time delay, so $\phi_m(f) = 2\pi f L/2$. Type-I filters are a good choice due to their versatility [42]. Consequently, the amplitude function can be written in the form

$$A_m(f) = \sum_{n=0}^{L/2} \widetilde{b}_{n,m} cos(2\pi f n) \tag{22}$$

where

$$\widetilde{b}_{n,m} = \begin{cases} b_{L/2,m} & n = 0 \\ 2b_{L/2-n,m} & 1 \le n \le L/2\,. \end{cases} \tag{23}$$

Let Φ denote the frequency range of interest. We uniformly discretize the frequency space and introduce K frequency bins $\{f_k\}_1^K \in \Phi$. We denote $\boldsymbol{b}_m$ as a vector of length $(L/2+1)$ containing the coefficients of the m-th ring, and $\boldsymbol{B}$ as a $(L/2+1)\times M$ matrix containing the coefficients of all rings, that is,

$$\boldsymbol{b}_m = \left(b_{0,m}, ..., b_{L/2,m}\right)^T \tag{24}$$

$$\boldsymbol{B} = (\boldsymbol{b}_1, ..., \boldsymbol{b}_M)\ . \tag{25}$$

We arrange the cosines values at frequency f in the vector $\boldsymbol{g}(f)$ of length $(L/2+1)$, and the values across all frequency bins in the $(L/2+1)\times K$ matrix $\boldsymbol{G}$, that is,

$$\boldsymbol{g}(f) = \left[1, 2\cos(2\pi f), ..., 2\cos(2\pi f L/2)\right]^T \tag{26}$$

$$\boldsymbol{G} = \left[\boldsymbol{g}(f_1), ..., \boldsymbol{g}(f_K)\right]\ . \tag{27}$$

Then, the amplitude function in matrix form, evaluated over the frequency grid, is given by

$$\boldsymbol{A} = \boldsymbol{B}^T \boldsymbol{G} \tag{28}$$

where $\boldsymbol{A}$ is a $M\times K$ matrix with entries holding $(\boldsymbol{A})_{k,m} = A_m(f_k)$.

2) Optimization Constraints: We present a set of constraints that should be considered while designing CB beamformers.

The first constraint restricts the FIR coefficients to the class of Type-I FIR filters and the amplitude response to be real-valued:

$$\mathcal{C}_1\ :\ \boldsymbol{A} = \boldsymbol{B}^T \boldsymbol{G}\,. \tag{29}$$

The second is the well-known distortionless response constraint, which ensures that any signal arriving from the desired direction will pass the beamformer without distortion, given by

$$\underline{\boldsymbol{h}}^T(f_k)\, \boldsymbol{T}^T \boldsymbol{d}(f_k, \theta_d) = 1,\ \forall f_k \in \Phi \tag{30}$$

Since we restrict ourselves to Type-I FIR filters, by (21), the filters frequency response can be expressed as

$$\underline{\boldsymbol{h}}(f_k) = \boldsymbol{a}_k e^{-j2\pi f L/2} \tag{31}$$

where $\boldsymbol{a}_k$ denotes the k-th column of the matrix $\boldsymbol{A}$. All filters share the same continuous linear phase response (pure delay) which by the commutative property of LTI systems can be applied after the summation part in Fig. 2, resulting

$$\mathcal{C}_2\ :\ (\boldsymbol{T}\boldsymbol{a}_k)^T \boldsymbol{d}(f_k, \theta_d) = 1,\ \forall f_k \in \Phi, \tag{32}$$

The beamformer aims to maintain CB across a large frequency range. Let Θ_{BW}, Φ_{BW} denote the angles and frequencies that cover the mainlobe region, respectively. We define the matrix $\boldsymbol{B}^{BW}$ containing the samples of the beampattern power over the grid as

$$\left(\boldsymbol{B}^{BW}\right)_{k,i} = \mathcal{B}\left[(\boldsymbol{T}\boldsymbol{a}_k), \theta_i\right] \tag{33}$$

where $k \in [1, |\Phi_{BW}|]$ and $i \in [1, |\Theta_{BW}|]$. Hence, a CB can be achieved by restricting the magnitude to be greater or equal to the magnitude at the mainlobe region, expressed as

$$\mathcal{C}_3 \ : \ \boldsymbol{B}^{BW} \geq A_{BW}, \tag{34}$$

where A_{BW} marks the -3 dB amplitude. In addition, the maximal beampattern fluctuation within the mainlobe region is constrained to be less than δ, that is,

$$\mathcal{C}_4 \ : \ \max \left| \boldsymbol{B}^{BW} - \mathbf{1}_{|\Phi_{BW}|} \otimes \boldsymbol{B}^{BW}_{|\Phi_{BW}|} \right| \leq \delta, \tag{35}$$

where $\boldsymbol{B}^{BW}_{|\Phi_{BW}|}$ is the $|\Phi_{BW}|$-th row of $\boldsymbol{B}^{BW}$, i.e., the beampattern of the highest frequency in the mainlobe region serving as a reference beampattern.

Furthermore, to avoid negative amplification values and improve robustness, a fifth constraint on the amplitude is added:

$$\mathcal{C}_5 \ : \ 0 \leq \boldsymbol{a}_k \leq 1, \ \forall k \in [1, K] \ . \tag{36}$$

3) Objective Function: Under the distortionless constraint in (32), the broadband DF and WNG can be expressed, respectively, as

$$\mathcal{D} = \sum_{k=1}^{K} \left[\left(\boldsymbol{T}\boldsymbol{a}_k \right)^T \boldsymbol{\Gamma} \left(f_k \right) \boldsymbol{T}\boldsymbol{a}_k \right]^{-1} \tag{37}$$

and

$$\mathcal{W} = \sum_{k=1}^{K} \left[\left(\boldsymbol{T}\boldsymbol{a}_k \right)^T \boldsymbol{T}\boldsymbol{a}_k \right]^{-1} . \tag{38}$$

We suggest the combination of the two as an objective function for the minimization problem, which is given by

$$\alpha \mathcal{D}^{-1} + (1 - \alpha) \mathcal{W}^{-1} \tag{39}$$

where α is a constant between 0 and 1, controlling the tradeoff between DF and WNG. A bigger α makes the DF more significant.

To sum up, the CB FIR-beamformer for a given CRA configuration can derived by solving the following CQP optimization problem:

$$\begin{aligned} \min_{\boldsymbol{A}, \boldsymbol{B}} \quad & \alpha \mathcal{D}^{-1} + (1 - \alpha) \mathcal{W}^{-1} \\ \text{s.t.} \quad & \mathcal{C}_1, \mathcal{C}_2, \mathcal{C}_3, \mathcal{C}_4, \mathcal{C}_5 \, . \end{aligned} \tag{40}$$

B. Genetic Algorithm

GA is a stochastic optimization technique inspired by natural selection, where a population of solutions evolves to solve complex problems efficiently.

In this paper, a candidate solution is a vector $\boldsymbol{r} = (R_1, ..., R_M)^T$ containing M real-valued ring radii, lying in the interval $[R_{min}, R_{max}]$. All solutions are normalized to have values between 0 and 1, and referred to as chromosomes. Without loss of generality, we assume the genes in a chromosome are sorted in ascending order. Next, we describe the main stages of the GA.

1) Initial Population: An initial population of chromosomes $\{\boldsymbol{x}_i\}_{i=1}^{N_{pop}}$ is generated by

$$\boldsymbol{x}_i = \boldsymbol{x}_{un} + \boldsymbol{n}_i \tag{41}$$

where $\boldsymbol{x}_{un}$ is the uniform solution of N_{genes} evenly spaced points in the $[0, 1]$ interval, and $\boldsymbol{n}_i$ is a $N_{genes} \times 1$ white Gaussian noise vector, with zero mean and standard deviation of σ_{pop}.

2) Fitness Calculation: The fitness of a chromosome describes how good is the solution. We use the negative of the cost obtained by the CQP optimization problem defined in (40) as the fitness where the fitness of the non-solvable chromosomes is set to the lowest fitness in the population. Next, the fitness values are scaled using the rank-scaled (RS) [43] technique, which scale the fitness values by their rank ordering preventing premature convergence.

3) Elitism: To ensure that the best solution won't be lost, we use the elitism strategy by passing the N_{elite} best chromosomes directly to the next generation.

4) Selection: Choosing the most fit parent chromosomes for reproduction is done using the stochastic universal sampling (SUS) [44] technique. In this technique, the chromosomes are chosen by one spinning of a roulette wheel with sections proportional to the fitness values and multiple equally spaced selection points, giving weaker solutions a chance to be chosen.

5) Crossover: Every two parents produce a child by combining their genetics using the extended intermediate crossover (EIC) [45] operator. Let $\boldsymbol{x}$ and $\boldsymbol{y}$ be two parent chromosomes. Then, a child chromosome is produced by

$$\boldsymbol{z} = \boldsymbol{x} + \boldsymbol{\alpha} \circ (\boldsymbol{y} - \boldsymbol{x}) \tag{42}$$

where $\boldsymbol{\alpha}$ is a random vector with elements uniformly distributed in the $[-0.25, 1.25]$ interval. The solutions are generated in a slightly larger hypercube, allowing the exploration of new solutions.

6) Mutation: Mutation allows the algorithm to explore new solutions and divert from converging to popular solutions. We use the dynamic multi-nonuniform mutation (DMNUM) [46] which decreases the mutation search interval as time progresses. Let $\boldsymbol{x}$ be a parent chromosome and $\boldsymbol{z}$ the produced child. We first generate a random vector $\boldsymbol{p}$ of length N_{genes} with elements uniformly distributed in the $[0, 1]$ interval. A gene is chosen to mutate if its probability is lower than the mutation probability p_{mu}^{gene}. Next, we iterate in random order over the chosen genes and apply the following mutation operation:

$$z_i = \begin{cases} x_i + [x_{i-1} - x_i] \, f(g) \, , & w.p. \ 0.5 \\ x_i - [x_i - x_{i+1}] \, f(g) \, , & w.p. \ 0.5 \end{cases} \tag{43}$$

$$f(g) = r \left(1 - \frac{g}{G_{max}} \right)^{\gamma} \tag{44}$$

where r is a uniform random number in the $[0, 1]$ interval, g is the current generation, G_{max} is the maximum number of generations and γ is a shape parameter. In the boundaries we use $x_0 = 0$ and $x_{N_{genes}+1} = 1$.

The algorithm terminates when the fitness of the fittest member does not change over a certain number of generations or when it reaches the maximal number of generations. To ensure that the individuals meet the constraints, we repair them by clipping and sorting after each operator.

The steps of the hybrid approach CB FIR beamformer are summarized in Algorithm 1.

Algorithm 1 Hybrid Genetic Algorithm

```
Generate initial population of size N_pop.
for i = 1 to N_gen do
    for j = 1 to N_pop do
        Evaluate fitness by solving (40).
    end for
    Scale fitness with RS.
    if convergence satisfied then
        break.
    end if
    Transfer N_elite best individuals to next generation.
    Select 2(N_pop − N_elite) individuals with SUS.
    for j = 1 to (N_pop − N_elite) do
        Apply EIC (42).
        Apply DMNUM (43) w.p. p_mu.
        Repair individuals.
    end for
    Replace the old population with the next generation.
end for
return best individual.
```

IV. Experimental Results

In this section, we provide a few simulation results examining the performance of the proposed approach compared to the state-of-the-art approach suggested by Kleiman [40]. In Section IV-A, the simulations demonstrate the advantages of the proposed CQP optimization for designing CB beamformers for a given CRA configuration. In Section IV-B, the simulations show the hybrid approach's advantage in computation time.

All simulations consider the design of a CB beampattern obtaining a beamwidth of $\theta_{BW} = 30°$ measured at amplitude $A_{BW} = 1/\sqrt{2}$ over the range of frequencies $[0, 8]$ kHz. The DoA of the desired signal is $\theta_d = 0$. The optimization problems were implemented in MATLAB using the CVX toolbox [47] and the MOSEK solver, and conducted on a Xeon E5-2697V4 CPU @ 2.3 GHz of Intel with 128GB of RAM. The source code for this paper can be found at. [1]

A. Constant-Beamwidth Beamformer Design

In this section, we consider the design of a CB FIR beamformer for a given CRA configuration. The chosen CRA configuration is a non-uniform CRA consisting of $M = 5$ rings, with radii $R_m = (2, 4.8, 8.1, 13.9, 25)^T$ cm, containing $N_m = (6, 15, 17, 19, 19)^T$ microphones, the same as that of Kleiman [40].

[1] https://github.com/PeretzOrel/CB-EL-CRA

1) Influence of α: The beampatterns power as a function of frequency and elevation for $\alpha = 1, 0.3, 0$ and $L = 32$ are shown in Figures 3(a)-(c), respectively. The overlayed dashed line is the half-power of the mainlobe. We can observe that the beamwidth is constant over the entire desired frequency range $\Phi_{BW} = [1.2, 8]$ kHz and mainlobe region $\Theta_{BW} = [-15°, 15°]$. The beamformer weights as a function of frequency applied to the rings for $\alpha = 1, 0.3, 0$ and $L = 32$ are shown in Figures 3(d)-(f), respectively. The choice of $\alpha = 1$, shown in Figures 3(a),(d), yields the maximum DF CB beamformer. We can see that the sidelobe level is low compared to the others, which is desired to reduce diffuse noise. Moreover, the produced filters are band-pass in nature. As the frequency increases, the inner rings dominate, while the outer ones become less dominant. The choice of $\alpha = 0$, shown in Figures 3(c),(f), yields the delay-and-sum CB beamformer. The produced filters are low-pass in nature. As the frequency decreases, more rings participate in the beamforming process, which can be thought of as beamforming with discrete pistons. In the low-frequency region, all the rings are active, which is desirable for reducing the microphone's inner white noise. For the choice of $\alpha = 0.3$, shown in Figures 3(b),(e), we get a compromise between the two beamformers above. The produced filters are band-pass in nature, with more extensive support toward the low frequencies, increasing the number of microphones participating in the beamforming process and reducing the microphone's inner white noise. For more on the tradeoff between beamwidth, radii, and frequency using discrete rings and pistons, the reader is referred to [33]. Overall, the definition of a single optimization problem, optimizing the FIR coefficients of all rings jointly, has several advantages. First, the design process is straightforward, produces smooth and continuous FIR filter responses, and does not require a pre-processing step, as suggested in Kleiman [40]. Second, the filter weights of different rings are dependent, and the ripples are coordinated, resulting in better beamwidth consistency, as shown in the following subsections.

Figures 4(a)–(b) show the DF and WNG as a function of frequency obtained by Kleiman [40] and the proposed approach for $\alpha = 1, 0.3, 0.15, 0$ and $L = 32$. The choice of $\alpha = 1$ yields the maximum DF CB beamformer, which maximizes the DF. The proposed beamformer attains slightly higher DF and WNG for most frequencies due to the direct and joint filter design. For the choice of $\alpha = 0$, we get the delay-and-sum CB beamformer, which maximizes the WNG. The suggested objective function allows a tradeoff between WNG and DF, which can be observed for $\alpha = 0.15, 0.3$. A bigger α improves the DF at the expense of the WNG. One can see that the choice of $\alpha = 0.3$ can be picked as a good compromise between WNG and DF. By allowing a maximal reduction of 0.5 dB in the DF, we improve the WNG by more than 1 dB in the low-frequency region and a maximal improvement of about 3dB at $f = 1.8$ kHz.

Figure 4(c) illustrates the beamwidth as a function of frequency obtained by Kleiman [40] and the proposed approach for $\alpha = 1, 0.3, 0.15, 0$ and $L = 32$. The mean and standard deviation of the beamwidth can measure the beamwidth consistency. Both approaches maintain an approximately CB

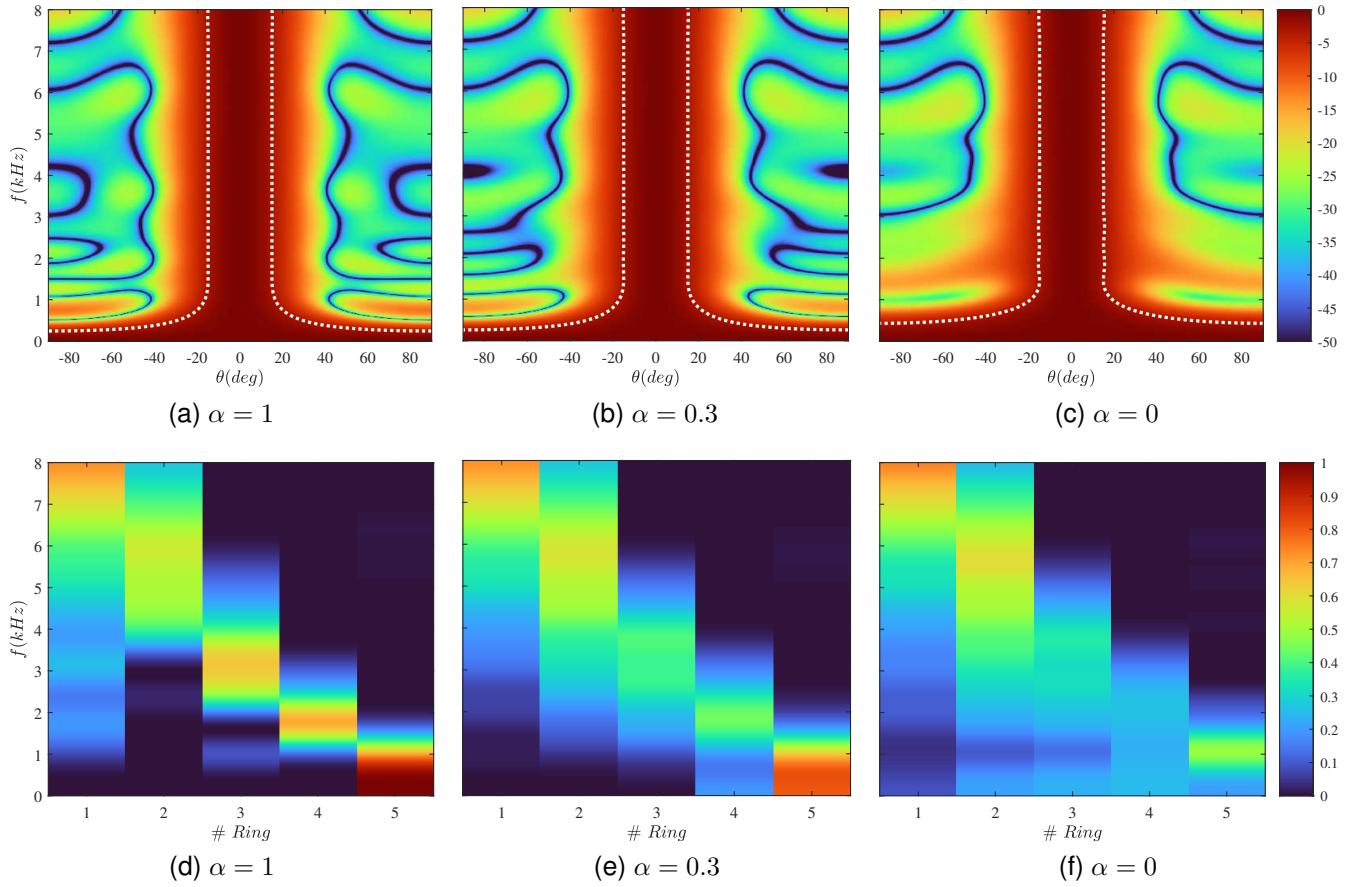

Fig. 3. (a-c) Beampatterns of the proposed beamformer for a non-uniform CRA with $M = 5$ rings and $L = 32$ filter taps. The overlayed dashed line is the half-power contour of the mainlobe. (d-f) Weight values are applied to the rings at each frequency.

of about 30° over the desired frequency range $[1.2, 8]$ kHz. Kleiman's approach [40] has high ripples that break the constraint of the beamwidth (to be larger than $\theta_{BW} = 30°$) while the proposed approach has low ripples and holds the constraints. The proposed approach obtains better beamwidth consistency due to the direct and joint design of the FIR coefficients.

2) Influence of L: The DF, WNG, and beamwidth as a function of frequency obtained by Kleiman [40] and the proposed beamformer for $\alpha = 1, 0.3, 0.15, 0$ and $L = 20$ are shown in Fig. 5. Compared to the results of $L = 32$ shown in Fig. 4, we notice that a smaller L damages the flexibility of the proposed approach. The maximal gain in the low-frequency region is reduced to maintain the constant beamwidth constraint. In addition, both approaches have higher ripples.

3) Sidelobe Level Comparison: The sidelobe level is another important performance measure. A beamformer with a low sidelobe level can suppress interference better. The beampatterns at different frequencies in the range of $[1.4, 7.6]$ kHz obtained by the proposed beamformer with $\alpha = 1$ and Kleiman's approach [40] for $L = 32$ are shown in Fig. 6. The solid line marks the sidelobe level. The SLL of the proposed approach is -22.2 dB, which is lower by more than 3 dB than Kleiman's SLL, which is -18.6 dB.

Table I summarizes the above performance measures for the different parameters. The SLL, beamwidth mean, and standard deviation were measured over $[1.4, 7.6]$ kHz. We can notice the tradeoff between the DF and WNG, controlled by α. A bigger α makes the DF more significant, and vice versa. In addition, the proposed approach has better beamwidth consistency (lower standard deviation) for the same number of filter taps. In general, the proposed approach achieves better performance with fewer filter taps.

B. Hybrid Approach

This section considers the joint design of both the beamformer coefficient and the ring radii.

The allowed radii lie between $R_{min} = 0$ cm and $R_{max} = 25$ cm. The population size is set to $N_{pop} = 100$, and the number of elite individuals to $N_{elite} = 0.1N_{pop}$. In each generation, we apply the crossover operation over $2(N_{pop} - N_{elite})$ individuals. The mutation operation is applied to the offspring with a probability $p_{mu} = 0.2$. The Gaussian noise standard deviation used for the initial population generation is $(R_{max} - R_{min})/5(M - 1)$. The parameters of DMNUM [46] are $\gamma = 2$ for the shape parameter, $p_{mu}^{gene} = 0.2$ for the mutation probability of the genes, and $N_{gen} = 100$ for the maximal number of generations. The cost function of the individuals is evaluated in parallel using the MATLAB parallel toolbox.

Figures 7(a)–(b) show the DF and WNG of the proposed hybrid approach as a function of frequency for $\alpha = 1, 0.3, 0.15, 0$

TABLE I
PERFORMANCE MEASURES COMPARISON FOR DIFFERENT PARAMETER CHOICES

Approach	L	α	$\mathcal{D}$(dB)	$\mathcal{W}$(dB)	$MEAN\{\theta^\circ{}_{BW}\}$	$STD\{\theta^\circ{}_{BW}\}$	SLL(dB)
Proposed	20	1	12.7	14.6	30.2	0.18	-23.7
	20	0.3	12.6	15.3	30.2	0.24	-22.3
	20	0.15	12.5	15.6	30.3	0.34	-20.1
	20	0	12.2	15.7	30.4	0.34	-13.7
	32	1	12.7	14.4	30.02	0.05	-22.2
	32	0.3	12.6	15.3	30.03	0.08	-22.4
	32	0.15	12.5	15.7	30.05	0.09	-21
	32	0	12.1	16.2	30.2	0.3	-14.3
Kleiman [40]	20	-	12.7	14.1	30.08	0.48	-19
	32	-	12.7	14.1	30.06	0.4	-18.6

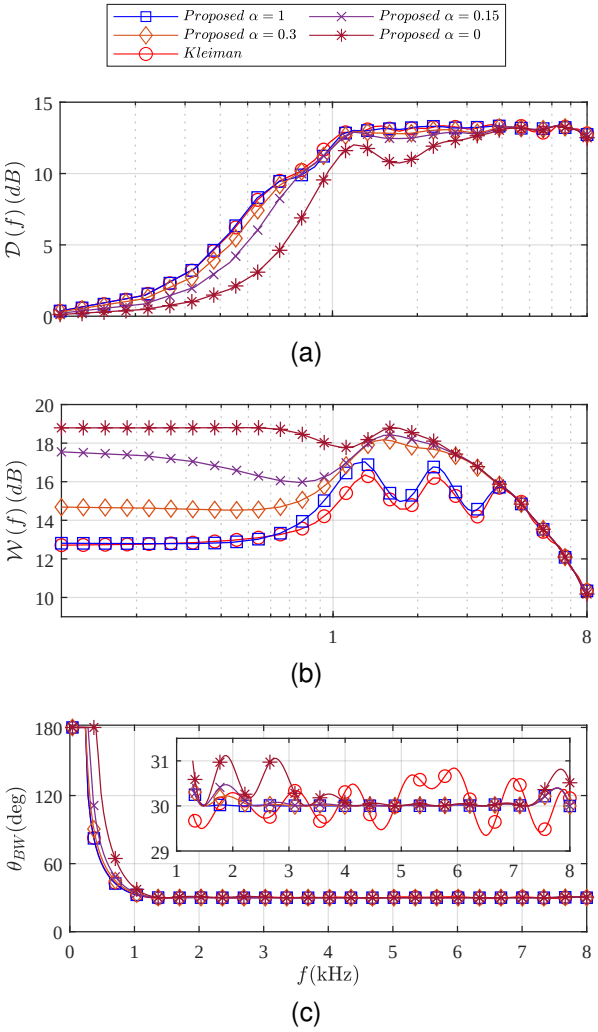

Fig. 4. Performance measures of the proposed beamformer with $\alpha = 1$ (square), $\alpha = 0.3$ (diamond), $\alpha = 0.15$ (cross), $\alpha = 0$ (asterisk), and Kleiman [40] (circle) for $L = 32$ filter taps. (a) DF, (b) WNG, and (c) Beamwidth θ_{BW}, as a function of frequency.

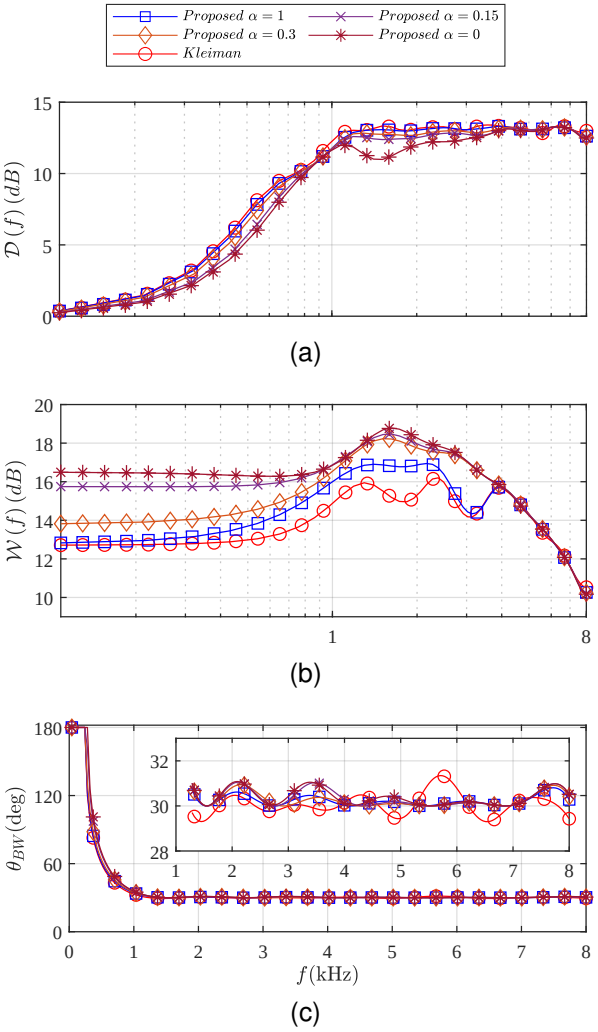

Fig. 5. Performance measures of the proposed beamformer with $\alpha = 1$ (square), $\alpha = 0.3$ (diamond), $\alpha = 0.15$ (cross), $\alpha = 0$ (asterisk), and Kleiman [40] (circle) for $L = 20$ filter taps. (a) DF, (b) WNG, and (c) Beamwidth θ_{BW}, as a function of frequency.

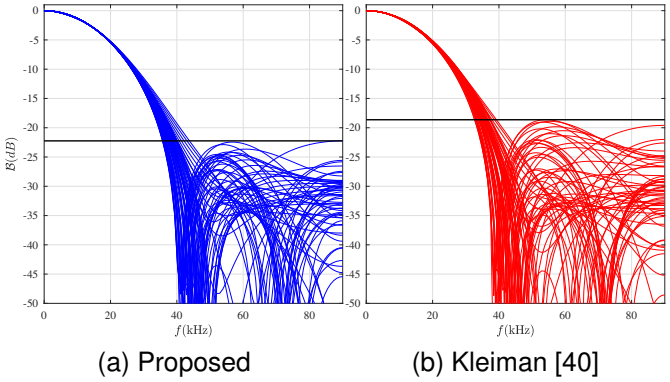

Fig. 6. Beampatterns at different frequencies in range $[1.4, 7.6]$ kHz with $L = 32, \alpha = 1$. The solid line marks the sidelobe level.

TABLE II
PRODUCED SOLUTIONS OF THE HYBRID APPROACH FOR DIFFERENT α CHOICES

α	R_m	N_m
1	$(2, 4.7, 7.9, 14.7, 25)^T$	$(6, 14, 18, 18, 11)^T$
0.3	$(1.7, 3.7, 6.2, 13, 24.5)^T$	$(6, 12, 17, 20, 19)^T$
0.15	$(2, 3.7, 6.1, 13, 24.8)^T$	$(7, 12, 17, 20, 20)^T$
0	$(2, 3.4, 3.7, 8.8, 23.8)^T$	$(7, 11, 12, 27, 28)^T$

and $L = 32$. For each α we get different ring radii and weights optimizing the cost objective in (40). The produced solutions are summarized in Table II. As α increases the broadband WNG in (40) becomes more dominant and the algorithm prefers weights with larger support resulting by (3) more elements in each ring which reduces the inner white noise of the microphones. Compared to Fig. 4 where the ring radii and number of microphones per ring were fixed, we get DF and WNG with higher dynamic range resulting from the optimization of the ring radii.

Figure 7(c) illustrates the beamwidth as a function of frequency obtained by the proposed hybrid approach for $\alpha = 1, 0.3, 0.15, 0$ and $L = 32$. The proposed hybrid approach maintains an approximately CB of about $30°$ over the desired frequency range $[1.2, 8]$ kHz for all α values.

Figure 8 illustrates the algorithm convergence, i.e., the cost value as a function of the generation number obtained by the proposed hybrid approach for $L = 32$ and $\alpha = 1$. The solid line and the shaded area are the mean and standard deviation of the cost over 100 independent MC runs, respectively. As the number of generations increases, the cost value converges to 7 dB with higher confidence. The best solution produced by a random run is $(2, 4.6, 7.4, 13.5, 25)$ cm, which is quite similar to the solution produced by Kleiman [40]. The average computation time of a single generation is 22 seconds, and for a whole run, it is 36 minutes. While the proposed hybrid approach takes about 36 minutes to run, Kleiman [40] runs for about 8 hours, almost two orders of magnitude more than the proposed approach. If a specific cost value is satisfactory, the proposed approach can stop before N_{gen}, resulting in a faster runtime.

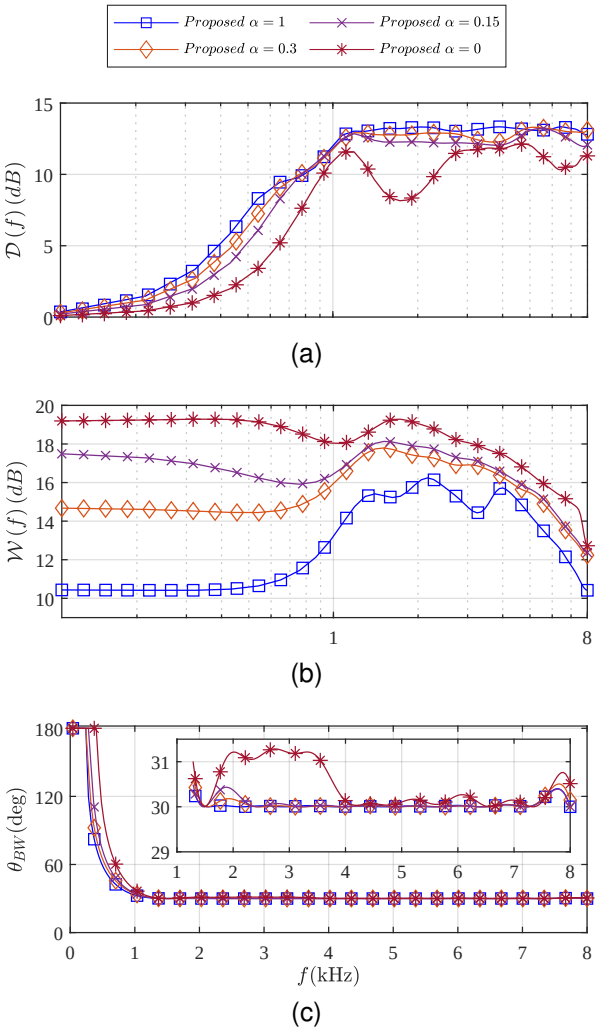

Fig. 7. Performance measures of the proposed hybrid approach with $\alpha = 1$ (square), $\alpha = 0.3$ (diamond), $\alpha = 0.15$ (cross) and $\alpha = 0$ (asterisk) for $L = 32$ filter taps. (a) DF, (b) WNG, and (c) Beamwidth θ_{BW}, as a function of frequency.

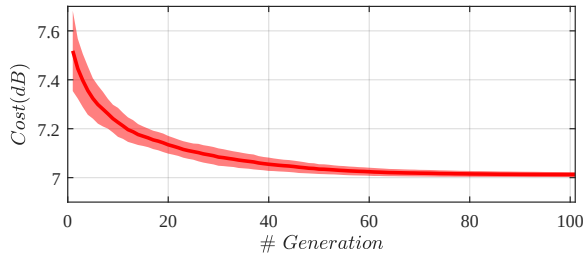

Fig. 8. Convergence plot. Cost value versus the number of generations obtained by the proposed hybrid approach. The solid line and the shaded area are the mean and standard deviation of the cost over 100 MC runs, respectively.

V. Conclusions

We have introduced a hybrid approach for designing a CB FIR beamformer with CRAs. The design optimizes the ring radii and the FIR beamformer coefficients, achieving superior performance. First, we defined a CQP optimization problem maintaining CB over an extensive range of frequencies for a given CRA configuration. Then, we proposed a hybrid approach to optimize the ring radii with a genetic algorithm utilizing the above convex problem as its cost and exploiting the partial convexity of the problem. Simulations show that the proposed approach provides a flexible solution for a good compromise between WNG and DF. In addition, it demonstrates improved performance in WNG, SLL, and beamwidth consistency with reasonable computational complexity. Future research may focus on different array geometries, optimization of clusters of rings, and testing the proposed design in the presence of mismatch errors, like element spacing errors.

References

[1] B. Van Veen and K. Buckley, "Beamforming: a versatile approach to spatial filtering," *IEEE ASSP Mag.*, vol. 5, no. 2, pp. 4–24, Apr. 1988.

[2] H. L. Van Trees, *Optimum Array Processing: Part IV of Detection, Estimation, and Modulation Theory*. New York, NY, USA: Wiley, 2002.

[3] J. Benesty, I. Cohen, and J. Chen, *Fundamentals of Signal Enhancement and Array Signal Processing*. Hoboken, NJ, USA: Wiley, 2018.

[4] M. Brandstein, D. Ward, A. Lacroix, and A. Venetsanopoulos, Eds., *Microphone Arrays: Signal Processing Techniques and Applications*. Berlin, Germany: Springer, 2001.

[5] I. Cohen, J. Benesty, S. Gannot, J. Benesty, and W. Kellermann, Eds., *Speech Processing in Modern Communication: Challenges and Perspectives*. New York, NY, USA: Springer, 2010.

[6] W. Liu and S. Weiss, "New class of broadband arrays with frequency invariant beam patterns," in *Proc. IEEE Int. Conf. Acoust., Speech, Signal Process.*, vol. 2, Montreal, QC, Canada, 2004, pp. ii–185–188.

[7] O. Rosen, I. Cohen, and D. Malah, "FIR-based symmetrical acoustic beamformer with a constant beamwidth," *Signal Process.*, vol. 130, pp. 365–376, 2017.

[8] Y. Buchris, A. Amar, J. Benesty, and I. Cohen, "Incoherent Synthesis of Sparse Arrays for Frequency-Invariant Beamforming," *IEEE/ACM Trans. Audio, Speech, Lang. Process.*, vol. 27, no. 3, pp. 482–495, Mar. 2019.

[9] T. Long, I. Cohen, B. Berdugo, Y. Yang, and J. Chen, "Window-Based Constant Beamwidth Beamformer," *Sensors*, vol. 19, no. 9, p. 2091, May 2019.

[10] A. Frank and I. Cohen, "Constant-Beamwidth Kronecker Product Beamforming With Nonuniform Planar Arrays," *Frontiers in Signal Process.*, vol. 2, 2022.

[11] W. Liu, "Design and implementation of a rectangular frequency invariant beamformer with a full azimuth angle coverage," *J. of the Franklin Inst.*, vol. 348, no. 9, pp. 2556–2569, Nov. 2011.

[12] G. Itzhak, I. Cohen, and J. Benesty, "Robust Differential Beamforming with Rectangular Arrays," in *Proc. 29th Eur. Signal Process. Conf.*, Dublin, Ireland, Aug. 2021, pp. 246–250.

[13] A. Frank, A. Ben-Kish, and I. Cohen, "Constant-Beamwidth Linearly Constrained Minimum Variance Beamformer," in *Proc. 30th Eur. Signal Process. Conf.*, Aug. 2022, pp. 50–54.

[14] G. Itzhak and I. Cohen, "Differential and Constant-Beamwidth Beamforming with Uniform Rectangular Arrays," in *Proc. Int. Workshop Acoust. Signal Enhancement*, Sep. 2022, pp. 1–5.

[15] G. Itzhak, J. Benesty, and I. Cohen, "Multistage approach for steerable differential beamforming with rectangular arrays," *Speech Communication*, vol. 142, pp. 61–76, Jul. 2022.

[16] V. P. Curtarelli and I. Cohen, "Constant-Beamwidth LCMV Beamformer with Rectangular Arrays," *Algorithms*, vol. 16, no. 8, p. 385, Aug. 2023.

[17] G. Itzhak and I. Cohen, "Region-of-Interest Oriented Constant-Beamwidth Beamforming with Rectangular Arrays," in *Proc. IEEE Workshop Appl. Signal Proc. Audio Acoust.*, Oct. 2023, pp. 1–5.

[18] J. Benesty, J. Chen, and I. Cohen, *Design of Circular Differential Microphone Arrays*. Berlin, Germany: Springer-Verlag, 2015.

[19] Y. Wang and Y. Yang, "A Flexible Method for Designing Frequency-Invariant Beamformers With Circular Sensor Arrays," *IEEE Access*, vol. 6, pp. 57 073–57 084, 2018.

[20] Y. Buchris, I. Cohen, and J. Benesty, "Frequency-Domain Design of Asymmetric Circular Differential Microphone Arrays," *IEEE/ACM Trans. Audio, Speech, Lang. Process.*, vol. 26, no. 4, pp. 760–773, Apr. 2018.

[21] S. C. Chan and H. H. Chen, "Uniform Concentric Circular Arrays With Frequency-Invariant Characteristic - Theory, Design, Adaptive Beamforming and DOA Estimation," *IEEE Trans. Signal Process.*, vol. 55, no. 1, pp. 165–177, Jan. 2007.

[22] W. Wang and S. Yan, "A flexible frequency-invariant beampattern synthesis method for concentric circular microphone arrays," in *Proc. IEEE Int. Conf. Acoust., Speech Signal Process.*, Sep. 2019, pp. 1–6.

[23] Y. Buchris, I. Cohen, J. Benesty, and A. Amar, "Joint Sparse Concentric Array Design for Frequency and Rotationally Invariant Beampattern," *IEEE/ACM Trans. Audio, Speech, Lang. Process.*, vol. 28, pp. 1143–1158, 2020.

[24] Y. Buchris, I. Cohen, and A. Amar, "Design of Frequency-Invariant Beamformers with Sparse Concentric Circular Arrays," in *Proc. IEEE Workshop Appl. Signal Proc. Audio Acoust.*, Oct. 2023, pp. 1–5.

[25] H. H. Chen, S. C. Chan, Z. G. Zhang, and K. L. Ho, "Adaptive Beamforming and Recursive DOA Estimation Using Frequency-Invariant Uniform Concentric Spherical Arrays," *IEEE Trans. Circuits Syst. I: Regular Papers*, vol. 55, no. 10, pp. 3077–3089, Nov. 2008.

[26] G. Itzhak and I. Cohen, "Differential constant-beamwidth beamforming with cube arrays," *Speech Communication*, vol. 149, pp. 98–107, 2023.

[27] G. Huang, J. Benesty, J. Chen, and I. Cohen, "Robust and steerable kronecker product differential beamforming with rectangular microphone arrays," in *Proc. IEEE Int. Conf. Acoust., Speech Signal Process.*, 2020, pp. 211–215.

[28] C. Mathews and M. Zoltowski, "Eigenstructure techniques for 2-D angle estimation with uniform circular arrays," *IEEE Trans. Signal Process.*, vol. 42, no. 9, pp. 2395–2407, Sep. 1994.

[29] M. I. Dessouky, H. Sharshar, and Y. Albagory, "Efficient Sidelobe Reduction Technique for Small-Sized Concentric Circular Arrays," *Prog. Electromagnetics Res.*, vol. 65, pp. 187–200, 2006.

[30] H. H. Chen, S. C. Chan, and K. L. Ho, "Adaptive Beamforming Using Frequency Invariant Uniform Concentric Circular Arrays," *IEEE Trans. Circuits Syst. I: Regular Papers*, vol. 54, no. 9, pp. 1938–1949, Sep. 2007.

[31] G. Huang, J. Chen, and J. Benesty, "Insights Into Frequency-Invariant Beamforming With Concentric Circular Microphone Arrays," *IEEE/ACM Trans. Audio, Speech, Lang. Process.*, vol. 26, no. 12, pp. 2305–2318, Dec. 2018.

[32] R. Sharma, I. Cohen, and B. Berdugo, "Controlling Elevation and Azimuth Beamwidths With Concentric Circular Microphone Arrays," *IEEE/ACM Trans. Audio, Speech, Lang. Process.*, vol. 29, pp. 1491–1502, 2021.

[33] A. Kleiman, I. Cohen, and B. Berdugo, "Constant-Beamwidth Beamforming with Concentric Ring Arrays," *Sensors*, vol. 21, no. 21, p. 7253, Jan. 2021.

[34] E. I. Elsaidy, M. I. Dessouky, S. Khamis, and Y. Albagory, "Concentric Circular Antenna Array Synthesis Using Comprehensive Learning Particle Swarm Optimizer," *Prog. Electromagnetics Res. Letters*, vol. 29, pp. 1–13, 2012.

[35] M. Carlin, G. Oliveri, and A. Massa, "Hybrid BCS-Deterministic Approach for Sparse Concentric Ring Isophoric Arrays," *IEEE Trans. Antennas Propag.*, vol. 63, no. 1, pp. 378–383, Jan. 2015.

[36] D. Jamunaa, G. Mahanti, and F. N. Hasoon, "Optimized inter-element arc spacing and ring radius in the synthesis of phase-only reconfigurable concentric circular array antenna using various evolutionary algorithms," *Electromagnetics*, vol. 40, no. 2, pp. 104–118, Feb. 2020.

[37] O. M. Bucci and D. Pinchera, "A Generalized Hybrid Approach for the Synthesis of Uniform Amplitude Pencil Beam Ring-Arrays," *IEEE Trans. Antennas Propag.*, vol. 60, no. 1, pp. 174–183, Jan. 2012.

[38] X. Zhao, Q. Yang, and Y. Zhang, "A Hybrid Method for the Optimal Synthesis of 3-D Patterns of Sparse Concentric Ring Arrays," *IEEE Trans. Antennas Propag.*, vol. 64, no. 2, pp. 515–524, Feb. 2016.

[39] J. Yang, F. Yang, P. Yang, and Z. Xing, "Synthesis of Clustered Concentric Ring Arrays Through Joint Optimization of Multi-Parameters," *IEEE Trans. Antennas Propag.*, vol. 71, no. 1, pp. 840–851, Jan. 2023.

[40] A. Kleiman, I. Cohen, and B. Berdugo, "Constant-Beamwidth Beamforming With Nonuniform Concentric Ring Arrays," *IEEE/ACM Trans. Audio, Speech, Lang. Process.*, vol. 30, pp. 1952–1962, 2022.

[41] L. C. Godara, "Application of the Fast Fourier Transform to Broadband Beamforming," *The Journal of the Acoustical Society of America*, vol. 98, no. 1, pp. 230–240, Jul. 1995.
[42] B. Porat, *A Course in Digital Signal Processing*. New York: Wiley, 1997.
[43] J. E. Baker, "Adaptive Selection Methods for Genetic Algorithms," in *Proc. 1st Int. Conf. Genetic Algorithms*. USA: L. Erlbaum Associates Inc., Jul. 1985, pp. 101–111.
[44] ——, "Reducing Bias and Inefficiency in the Selection Algorithm," in *Proc. 2nd Int. Conf. Genetic Algorithms*. USA: L. Erlbaum Associates Inc., Oct. 1987, pp. 14–21.
[45] H. Mühlenbein and D. Schlierkamp-Voosen, "Predictive Models for the Breeder Genetic Algorithm I. Continuous Parameter Optimization," *Evolutionary Computation*, vol. 1, no. 1, pp. 25–49, Mar. 1993.
[46] J. Yang, P. Yang, F. Yang, and Z. Xing, "A Hybrid Approach for the Synthesis of Nonuniformly Spaced and Excited Linear Arrays With Strict Element Spacing Constraints," *IEEE Trans. Antennas Propag.*, vol. 70, no. 7, pp. 5521–5533, Jul. 2022.
[47] M. Grant and S. Boyd, "CVX: Matlab Software for Disciplined Convex Programming, version 2.1," 2014. [Online]. Available: http://cvxr.com/cvx